Applied Chemical Engineering (2023) Volume 6 Issue 2
doi: 10.24294/ace.v6i2.2162

ORIGINAL RESEARCH ARTICLE

Phase equilibria in the Ag_8SiSe_6-Ag_8SiTe_6 system and characterization of the solid solutions $Ag_8SiSe_{6-x}Te_x$

Aynura Jabbar Amiraslanova[1], Kamala Naghi Babanly[2], Samira Zakir Imamaliyeva[2], Yusif Amrali Yusibov[1], Mahammad Baba Babanly[2,*]

[1] *Ganja State University, Ganja AZ-2000, Azerbaijan*

[2] *Institute of Catalysis and Inorganic Chemistry named after academician Murtuza Naghiyev, Baku AZ-1143, Azerbaijan*

*** Corresponding author:** Mahammad Baba Babanly, babanlymb@gmail.com

ABSTRACT

Due to polymorphism and complex crystal structure, compounds of the argyrodite family and phases based on them exhibit several interesting functional properties, such as thermoelectric, photoelectric, optical, as well as ionic conductivity for Cu^+ and Ag^+ cations. The paper presents the results of the study of phase equilibria in the Ag_8SiSe_6-Ag_8SiTe_6 system by DTA, XRD, and SEM methods. Refined data on the melting temperature (1278 K) and polymorphic transitions (315 K and 354 K) of the Ag_8SiSe_6 compound are presented. The crystallographic parameters of LT-Ag_8SiSe_6 (Cubic, *F*-43*m*, *a* = 1.0965 nm) and IT-Ag_8SiSe_6 (Cubic, $P4_232$, *a* = 1.0891 nm) are also determined. It has been established that the investigated system is quasi-binary and its phase diagram is characterized by the formation of a continuous series of substitutional solid solutions between HT-Ag_8SiSe_6 and Ag_8SiTe_6. This process is accompanied by a strong decrease in the temperatures of polymorphic transformations of Ag_8SiSe_6, which leads to the stabilization of the ion-conducting cubic phase at room temperature in the >10 mol% Ag_8SiTe_6 compositions area. The crystal lattice parameters of the synthesized solid solutions are calculated by indexing the powder diffraction patterns. The stabilization of the high-temperature cubic phase at room temperature achieved by us presents new opportunities for the development of environmentally friendly thermoelectrics and ion-electronic conductors based on silicon argyrodites with desired composition and properties.

Keywords: silver-silicon chalcogenides; argyrodite-like compounds; differential thermal analysis; X-ray diffraction analysis; phase equilibria; solid solutions; polymorphic transformation

ARTICLE INFO

Received: 25 May 2023
Accepted: 26 June 2023
Available online: 7 August 2023

1. Introduction

Silver and copper chalcogenides, due to their electronic, optical and mechanical properties, are good environmentally friendly materials for a wide range of applications, for example, as thermoelectric and photovoltaic materials, ionic conductors[1–7]. Recent studies show the promise of using them also in biomedicine[8,9] and for photoelectrochemical water splitting[10–12].

Among these materials, an important place is occupied by compounds with the general formula $A^I_8B^{IV}X_6$ (A^I-Cu, Ag; B^{IV}-Si, Ge, Sn; X-S, Se, Te) that belong to the argyrodite family. These compounds are of particular interest due to their thermoelectric properties[13–20], photosensitivity[21–23], and low-temperature phase transition[6,24]. These materials can be used in the production of hydrogen, as well as in a variety of applications such as ion-selective electrodes, solid-state electrolytes in various types of electric batteries,

electrochemical sensors, and displays[25–32]. According to some papers[14,17,31,32], the presence of mixed electronic-ionic conductivity is one of the significant factors that positively impact the thermoelectric characteristics of these materials.

A set of reliable data on phase equilibria and thermodynamic data play an important role in choosing the conditions for the directed synthesis of new materials[33–35]. Systems in which solid solutions are formed are of particular interest, since varying the composition can change the properties of the phases[36–39]. The constructed phase diagrams of such systems serve as the basis for choosing the composition of melts for growing single crystals of solid solutions of a given composition by the directed crystallization method.

Previously, the results of studies of systems composed of copper or silver chalcogenides and characterized by the formation of continuous or wide areas of solid solutions were presented[40–46].

In recent years, silicon-containing argyrodites, especially Ag_8SiSe_6 and Ag_8SiTe_6, have attracted particular interest as eco-friendly thermoelectric and ion-conducting materials[16,18,19].

In this work, in order to obtain new silicon argyrodites of variable composition, we studied phase equilibria in the Ag_8SiSe_6-Ag_8SiTe_6 system.

The initial compounds of the above-mentioned system have been studied in many works. The Ag_8SiSe_6 melts congruently. In various papers, very different values of the melting point of this compound are given. Thus, this compound melts at 1203 K[24,47]. In other papers, the following data are given: 1258 K[48], 1268 K[49]. The phase diagram presented by Jiang et al.[16] does not indicate a certain temperature of the distectics point, but only a possible melting temperature range (1203–1263 K).

The Ag_8SiSe_6 compound has at least 3 crystalline modifications[16,19,24,47]. The high-temperature (HT) modification, like all other compounds of the argyrodite family, crystallizes in a face-centered cubic structure (Sp.gr. *F*-43*m*) with complete disordering of the cationic sublattice. According to various authors, HT-Ag_8SiSe_6 has the following lattice periods: a = 1.097 nm[24,47], a = 1.09413(1) nm[19]. The intermediate modification (IT) has a simple-cubic structure (Sp.gr. $P2_13$[19] or $P4_232$ with a lattice constant a = 1.087 nm[24]). The IT-Ag_8SiSe_6 modification is characterized by partial localization of silver ions[19]. Data on the structure of the low-temperature modification (LT-Ag_8SiSe_6) are contradictory. LT-Ag_8SiSe_6 has a tetragonal structure (Sp.gr. *I*-4*m*2, a = 0.7706, b = 1.10141 nm[24,47]). However, Jiang et al.[16] noted that the powder diffraction pattern of LT-Ag_8SiSe_6 is poorly indexed in this structure. They showed that the diffractogram contains two series of reflections, and most of the peaks are indexed in the orthorhombic structure (Sp.gr $Pmn2_1$). Weak peaks near 33.5, 34.7 and 37.0 correspond to orthorhombic RT-Ag_2Se[16].

The Ag_8SiTe_6 melts congruently at 1143 K[24] and has two polymorphic transformations at 195 and 263 K[50]. The period of cubic lattice (Sp.gr. *F*-43*m* is a = 1.15225 nm[50]).

Based on the literature data, it can be assumed that continuous solid solutions can form between the high-temperature modification of HT-Ag_8SiSe_6 and Ag_8SiTe_6.

2. Materials and methods

For the synthesis of Ag_8SiSe_6 and Ag_8SiTe_6 compounds, the high-purity elements (at least 99.999 wt.% purity) were used. The synthesis was carried out in ampoules evacuated to 10^{-2} Pa. To avoid a reaction between silicon and the walls of the quartz ampoule, the inner walls of the tube were graphitized by pyrolysis of toluene.

Given the high vapor pressure of selenium at the melting point of Ag_8SiSe_6[51], this compound was synthesized in an in inclined two-zone furnace. Stoichiometric amounts of elementary components were loaded into a quartz ampoule (~13–15 cm long and ~1.5 cm in diameter), which, after evacuation and sealing, was placed in an inclined (~30°) tube furnace. Two-thirds of the ampoule was in the furnace, and the rest of

the upper part was outside the furnace. The furnace was heated to 1300 K. At the beginning of the experiment, selenium evaporates and accumulates in the upper “cold” zone of the ampoule, from where it returned to the lower “hot” zone again. To prevent the explosion of the ampoule due to overheating of the “cold” zone, the latter was cooled with water. As the components interacted, the amount of selenium in the upper part of the ampoule decreased, which could be observed visually. After the interaction of a larger mass of components, the ampoule was completely placed in the furnace.

Synthesis of the Ag_8SiTe_6 compound was carried out at 1200 K.

DTA and XRD analysis were used for the identification of the synthesized compounds.

Figure 1 presents the DTA data of the Ag_8SiSe_6 and Ag_8SiTe_6 compounds. As can be seen, these compounds melt at 1278 K and 1143 K. On the heating thermogram of the Ag_8SiSe_6 compound, there are also endothermic effects at 315 K and 354 K, corresponding to the polymorphic transitions. The data for Ag_8SiTe_6 compounds are in agreement with the literature[24]. According to our experimental data, the melting point of Ag_8SiSe_6 differs significantly from those presented by the authors[24,47,48] and is closer to the data of Piskach et al.[49]. The temperature of the low-temperature phase transition (315 K) coincides with the data of Gorochov[24] and Hofmann[47] while the temperature of the second one (354 K) is slightly lower than given by Studenyak et al.[30].

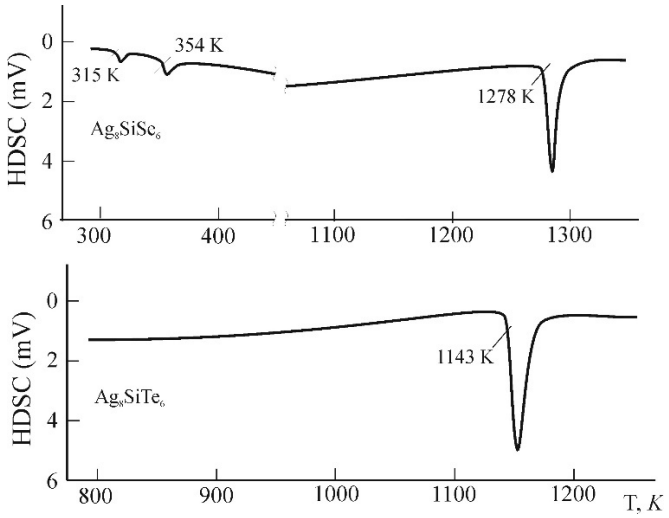

Figure 1. Heating DTA curves of the Ag_8SiSe_6 and Ag_8SiTe_6 compounds.

Intermediate samples of the studied system were prepared by melting stoichiometric amounts of pre-synthesized and identified compounds in evacuated quartz ampoules. The alloys were heated to 1300 K and kept at this temperature for about 1 h; then the furnace temperature was reduced to 800 K and the ampoules were kept in it for about 500 h. For some compositions, two series of alloys were prepared: the first series after annealing was quenched in ice water, and the second series of samples was slowly cooled in a furnace to room temperature.

Figure 2 shows the powder diffraction patterns of the synthesized compounds. The X-ray diffraction pattern of Ag_8SiTe_6 is in agreement with the literature data[24,52]. The diffraction pattern of Ag_8SiSe_6 is almost completely indexed in a simple-cubic lattice with Sp.gr. $P4_232$. Some non-indexed very weak reflection lines do not apply to Ag_2Se, $SiSe_2$, and initial elemental components. Taking into account the available literature data[16,19], it can be assumed that the synthesized sample is IT-Ag_8SiSe_6 with an insignificant part of LT-Ag_8SiSe_6. This assumption is supported by the DTA data, according to which the obtained sample has a clear isothermal melting peak, which is possible only if its composition coincides with the stoichiometry of Ag_8SiSe_6.

The obtained alloys were investigated by using DTA, XRD, and SEM methods.

The DTA curves were recorded using a NETZSCH 404 F1 Pegasus system with chromel-alumel thermocouples in the range of temperatures from room temperature to ~1400 K at a heating rate of 10 $K \cdot min^{-1}$ and standard uncertainty ±2°. Temperatures of thermal effects were taken mainly from the heating curves. But in some samples, thermal effects were taken from cooling curves to determine the onset of crystallization. As a reference material, in (429 K), Tl (576 K), Zn (692 K), Sb (904 K), KCl (1043 K), Ag (1236 K), as well as Cu (1358 K) with an accuracy of ±1° were used.

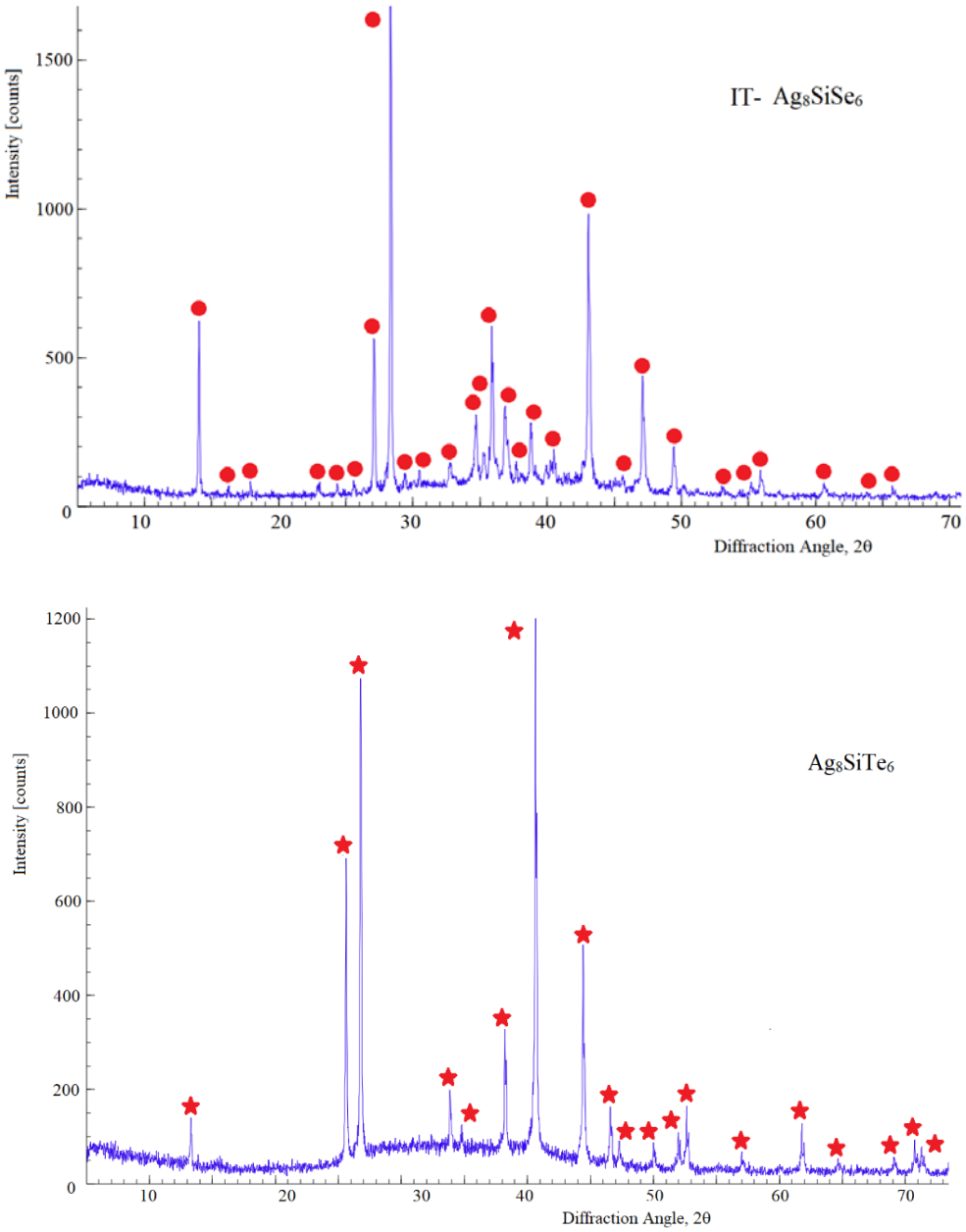

Figure 2. Powder diffraction patterns of the synthesized Ag_8SiSe_6 and Ag_8SiTe_6 compounds.

X-ray powder diffraction data were collected at room temperature using a Bruker D8 ADVANCE diffractometer (with Cu-Kα_1 radiation) within 2θ = 10° to 70°. The unit cell parameters were calculated by indexing powder patterns using Topas V3.0 software.

SEM-EDS analyses were done by Tescan Vega 3 SBH Scanning Electron Microscope equipped with Thermo Scientific Ultra Dry Compact EDS detector.

3. Results and discussion

Analysis of the powder diffraction patterns of both series of synthesized alloys with compositions of 10–90 mol% Ag_8SiTe_6 showed that they all have diffraction patterns characteristic for the HT-cubic *F*-43*m* space group. **Figure 3** shows powder diffractograms of alloys slowly cooled after annealing. As can be seen, all intermediate alloys have diffraction patterns that are qualitatively different from IT-Ag_8SiSe_6 and are similar to the diffraction pattern of Ag_8SiTe_6. Some shift of the reflection lines with increasing tellurium content towards smaller angles is associated with an increase in the lattice period during the formation of solid solutions.

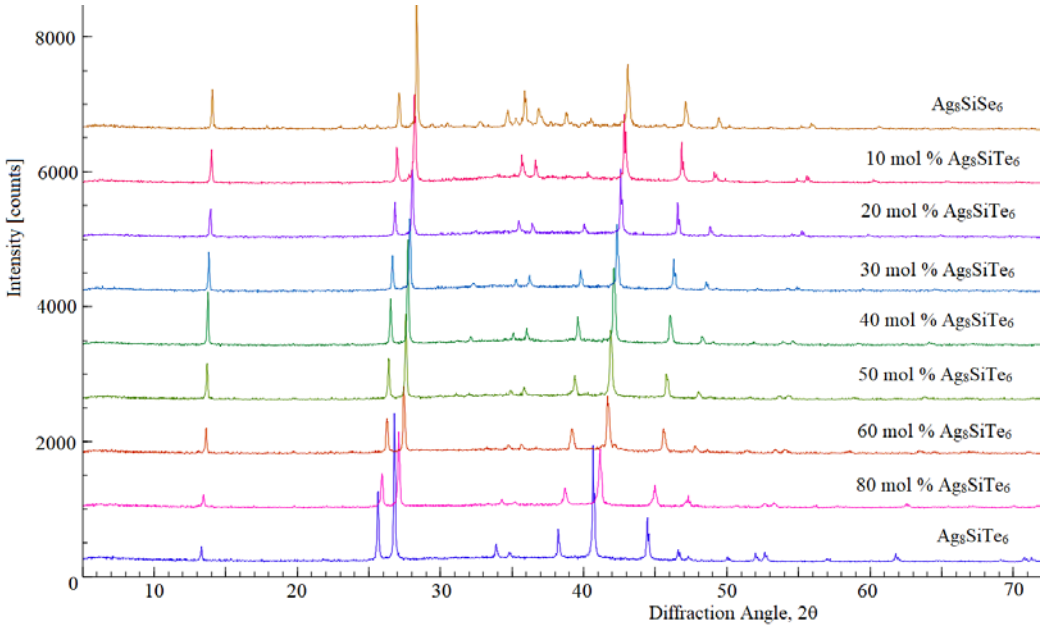

Figure 3. Powder diffractograms of some alloys of the Ag_8SiSe_6-Ag_8SiTe_6 system slowly cooled after annealing.

Table 1 presents the crystallographic data of slowly cooled after annealing and quenched from 800 K both initial compounds and alloys of the Ag_8SiSe_6-Ag_8SiTe_6 system, and **Figure 4** shows a graph of the concentration dependence of the cubic lattice period. As can be seen, for both series of alloys, the lattice period is an almost linear function of the composition, i.e., Vegard's law is obeyed. It should be noted that the values of the lattice constant of cubic phases at room temperature are somewhat smaller than those of alloys quenched from 800 K, which is apparently due to the thermal expansion of the crystal lattice of quenched samples compared to room temperature.

Table 1. Crystallographic parameters of phases in the Ag_8SiSe_6-Ag_8SiTe_6 system.

Composition, mol% Ag_8SiTe_6	**Syngony, Sp.gr., lattice parameters, nm**	
	Room temperature	**Quenched from 800 K**
Ag_8SiSe_6	Cubic, $P4_232$, a = 1.0891(3)	Cubic, *F*-43*m*, a = 1.0965(3)
10	Cubic, *F*-43*m*, a = 1.1018(3)	-" -, a = 1.1023(3)
20	-" -, a = 1.1070(4)	-" -, a = 1.1074(4)
40	-" -, a = 1.1175(3)	-" -, a = 1.1180(3)
50	-" -, a = 1.1230(4)	-
60	-" -, a = 1.1293(3)	-" -, a = 1.1298(3)
80	-" -, a = 1.1405(4)	-" -, a = 1.1411(4)
Ag_8SiTe_6	-" -, a = 1.1524(4)	-" -, a = 1.1528(3)

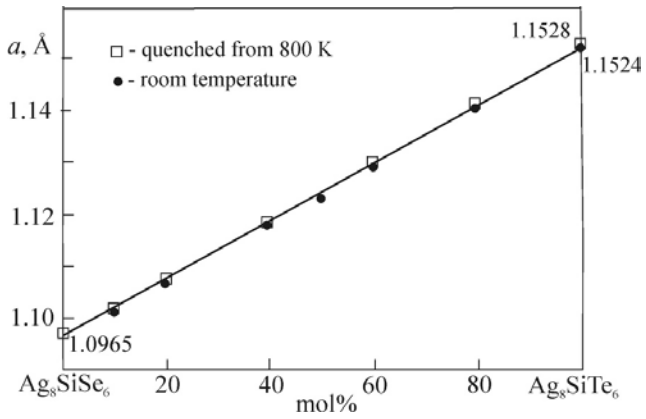

Figure 4. Dependence of the period of the cubic lattice on the composition for solid solutions of the Ag_8SiSe_6-Ag_8SiTe_6 system.

Table 2 presents the DTA data of the heating curves for the alloys slowly cooled after annealing. **Figure 5** shows the phase diagram constructed based on these data. As can be seen, the system is quasi-binary and is characterized by the formation of a continuous series of solid solutions (γ-phase) between HT-Ag_8SiSe_6 and Ag_8SiTe_6. On the liquidus and solidus curves, the temperature changes monotonically between the melting points of initial compounds, and the melting temperature range does not exceed 15°. On the DTA curves of the alloys, in contrast to pure Ag_8SiSe_6, we did not detect low-temperature thermal effects reflecting its polymorphic transitions. This, taking into account the XRD data, suggests that the formation of solid solutions is accompanied by a strong decrease in the temperatures of polymorphic transitions of Ag_8SiSe_6 (315 K and 354 K) and their transition to the temperature range below room temperature in the composition range of 0–10 mol% Ag_8SiTe_6.

Table 2. The DTA results for the alloys of the Ag_8SiSe_6-Ag_8SiTe_6 system.

Composition, mol% Ag_8SiTe_6	**Thermal effects, K**
Pure-Ag_8SiSe_6	315; 354; 1278
10	1262
20	1250–1264
40	1222–1237
50	1210–1225
60	1198–1212
80	1168–1278
90	1158–1165
Pure-Ag_8SiTe_6	1143

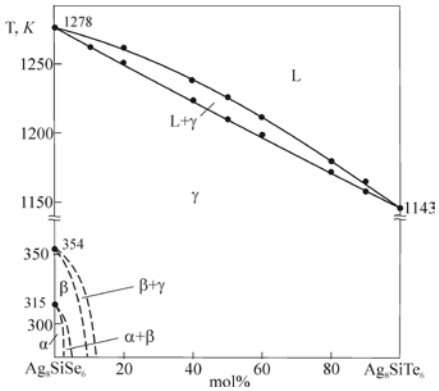

Figure 5. Phase diagram of the Ag_8SiSe_6-Ag_8SiTe_6 system.

The character of solid-phase equilibria in the Ag_8SiSe_6-Ag_8SiTe_6 system was also confirmed by the SEM method. It was shown that all synthesized samples are single-phase. **Figure 6** presents SEM-EDS data of annealed and slowly cooled alloy with a composition of 20 mol% Ag_8SiTe_6. As can be seen, this alloy is single-phase and its elemental composition practically coincides with the nominal $Ag_8SiSe_{4.8}Te_{1.2}$.

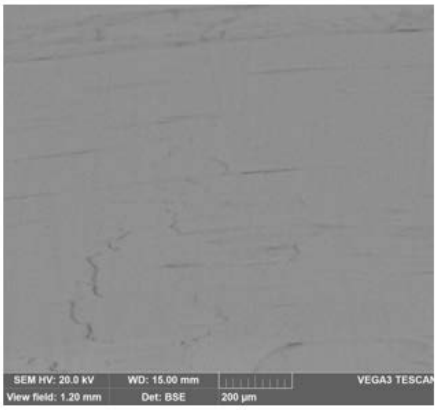

(A)

Element	Atomic %
Si K	6.65
Se K	32.04
Ag K	53.35
Te K	7.96
Sum	100

(B)

Figure 6. SEM-EDS data for the alloy with $Ag_8SiTe_{1.2}Se_{4.8}$ composition. **(A)** SEM image; **(B)** atomic composition of elements.

4. Conclusion

We present new data on phase equilibria in the Ag_8SiSe_6-Ag_8SiTe_6 system, obtained by DTA, XRD and SEM are presented. The temperatures of melting and polymorphic transitions, as well as the crystallographic parameters of the HT- and IT- modifications of the Ag_8SiSe_6 compound, for which contradictory literature data were available, are refined.

We have shown that the Ag_8SiSe_6-Ag_8SiTe_6 system is quasi-binary. Its T-x diagram in the high-temperature region is characterized by the formation of continuous solid substitution solutions between HT-Ag_8SiSe_6 and Ag_8SiTe_6. The formation of solid solutions is accompanied by a strong decrease in the temperatures of Ag_8SiSe_6 polymorphic transformations. This leads to the stabilization of the ion-conducting cubic phase with Sp.gr. *F*-43*m* at room temperature in a wide range of compositions (>10 mol% Ag_8SiTe_6). According to powder diffraction patterns, the crystal lattice parameters of the synthesized solid solutions were calculated. It is shown that the dependence of the cubic lattice period on the composition obeys Vegard's rule.

The obtained new data open up wide opportunities for obtaining environmentally friendly thermoelectrics and ion-electronic conductors based on silicon argyrodites with controlled composition and properties.

Funding

The work was supported by the Azerbaijan Science Foundation, Grant No. AEF-MCG—2022-1(42)-12/10/4-M-10.

Author contributions

Conceptualization, YAY; methodology, AJA and KNB; investigation, AJA and KNB; resources, SZI; data curation, YAY; writing—original draft preparation, AJA; writing—review & editing, KNB; visualization, SZI; project administration, MBB; funding acquisition, MBB.

Conflict of interest

The authors declare no conflict of interest.

References

1. Liu X, Lee S, Furdyna JK, et al. *Chalcogenide: From 3D to 2D and Beyond*. Elsevier; 2019.
2. Woodrow P. *Chalcogenides: Advances in Research and Applications*. Nova Science Publishers; 2018.
3. Alonso-Vante N. C*halcogenide Materials for Energy Conversion: Pathways to Oxygen and Hydrogen Reactions.* Springer; 2018.
4. Ahluwalia GK. *Applications of Chalcogenides: S, Se, and Te.* Springer-Verlag; 2016.
5. Scheer R, Schock HW. *Chalcogenide Photovoltaics: Physics, Technologies, and Thin Film Devices*. Wiley, VCH; 2011.
6. Babanly MB, Yusibov YuA, Abishev VT. *Ternary Chalcogenides on the Base of Copper and Silver* (Russian). Baku: Baku Girls University; 1993.
7. Mitra D, Kang ET, Neoh KG. Antimicrobial copper-based materials and coatings: Potential multifaceted biomedical applications. *ACS Applied Materials & Interfaces* 2020; 12(19): 21159–21182. doi: 10.1021/acsami.9b17815
8. Nieves LM, Mossburg K, Hsu JC, et al. Silver chalcogenide nanoparticles: A review of their biomedical applications. *Nanoscale* 2021; 13: 19306–19323. doi: 10.1039/D0NR03872E
9. Tee SY, Ponsfordm D, Lay CL, et al. Thermoelectric silver-based chalcogenides. *Advanced Science* 2022; 9(36): 2204624. doi: 10.1002/advs.202204624
10. Kumar M, Meena B, Subramanyam P, et al. Emerging copper-based semiconducting materials for photocathodic applications in solar driven water splitting. *Catalysts* 2022; 12(10): 1198. doi: 10.3390/catal12101198
11. Mensah-Darkwa K, Ampong DN, Agyekum E, et al. Recent advancements in chalcogenides for electrochemical energy storage applications. *Energies* 2022; 15(11): 4052. doi: 10.3390/en15114052
12. Ramasamy K, Gupta RK, Palchoudhury S, et al. Layer-structured copper antimony chalcogenides ($CuSbSe_xS_{2-x}$): Stable electrode materials for supercapacitors. *Chemistry of Materials* 2015; 27(1): 379–386. doi: 10.1021/cm5041166
13. Lin S, Li W, Pei Y. Thermally insulative thermoelectric argyrodites. *Materials Today* 2021; 48: 198–213. doi: 10.1016/j.mattod.2021.01.007
14. Schwarzmüller S, Souchay D, Günther D, et al. Argyrodite-type $Cu_8GeSe_{6-x}Te_x$ ($0 \leq x \leq 2$): Temperature-dependent crystal structure and thermoelectric properties. *Zeitschrift für anorganische und allgemeine Chemie* 2018; 644(2): 1915–1922. doi: 10.1002/zaac.201800453
15. Jiang B, Qiu P, Eikeland E, et al. Cu_8GeSe_6-based thermoelectric materials with an argyrodite structure. *Journal of Materials Chemistry C* 2017; 5: 943–952. doi: 10.1039/C6TC05068A
16. Jiang Q, Li S, Luo Y, et al. Ecofriendly highly robust Ag_8SiSe_6-based thermoelectric composites with excellent performance near room temperature. *ACS Applied Materials & Interfaces* 2020; 12(49): 54653–54661. doi: 10.1021/acsami.0c15877
17. Fan Y, Wang G, Wang R, et al. Enhanced thermoelectric properties of p-type argyrodites Cu_8GeS_6 through Cu. *Journal of Alloys and Compounds* 2020; 822: 153665. doi: 10.1016/j.jallcom.2020.153665
18. Charoenphakdee A, Kurosaki K, Muta H, et al. Ag_8SiTe_6: A new thermoelectric material with low thermal conductivity. *Japanese Journal of Applied Physics* 2009; 48: 011603. doi: 10.1143/JJAP.48.011603
19. Heep BK, Weldert KS, Krysiak Y, et al. High electron mobility and disorder induced by silver ion migration lead to good thermoelectric performance in the argyrodite Ag_8SiSe_6. *Chemistry of Materials* 2017; 29(11): 4833–4839. doi: 10.1021/acs.chemmater.7b00767
20. Shen X, Xia Y, Yang C, et al. High thermoelectric performance in sulfide-type argyrodites compound $Ag_8Sn(S_{1-x}Se_x)_6$ enabled by ultralow lattice thermal conductivity and extended cubic phase regime. *Advanced Functional Materials* 2020; 30: 2000526. doi: 10.1002/adfm.202000526
21. Semkiv I, Ilchuk N, Kashuba A. Photoluminescence of Ag_8SnSe_6 argyrodite. *Low Temperature Physics* 2022; 48(1): 12–15. doi: 10.1063/10.0008957
22. Brammertz G, Vermang B, ElAnzeery H, et al. Fabrication and characterization of ternary Cu_8SiS_6 and Cu_8SiSe_6 thin film layers for optoelectronic applications. *Thin Solid Films* 2016; 616: 649–654. doi: 10.1016/j.tsf.2016.09.049
23. Slade TJ, Gvozdetskyi V, Wilde JM, et al. A Low-temperature structural transition in canfieldite, Ag_8SnS_6, single crystals. *Inorganic Chemistry* 2021; 60(24): 19345–19355. doi: 10.1021/acs.inorgchem.1c03158
24. Gorochov O. Les composés Ag_8MX_6 (M = Si, Ge, Sn et X = S, Se, Te). *Bulletin de la Société Chimique de France* 1968; 101: 2263–2275.
25. Yang M, Shao G, Wu B, et al. Irregularly shaped bimetallic chalcogenide ag_8sns_6 nanoparticles as electrocatalysts for hydrogen evolution. *ACS Applied Nano Materials* 2021; 4(7): 6745–6751. doi: 10.1021/acsanm.1c00769
26. Yeh LY, Cheng KW. Modification of Ag_8SnS_6 photoanodes with incorporation of Zn ions for photo-driven hydrogen production. *Catalysts* 2021; 11(3): 363. doi: 10.3390/catal11030363
27. Ivanov-Shits AK, Murin IV. Ionika tverdogo tela. *Solid State Ionics* 2000; 1: 132.
28. Li L, Liu Y, Dai J, et al. High thermoelectric performance of superionic argyrodite compound Ag_8SnSe_6. *Journal of Materials Chemistry C* 2016; 4: 5806–5813. doi: 10.1039/C6TC00810K

29. Sardarly RM, Ashirov GM, Mashadiyeva LF, et al. Ionic conductivity of the Ag_8GeSe_6 compound. *Modern Physics Letters B* 2023; 36: 2250171. doi: 10.1142/S0217984922501718
30. Studenyak IP, Pogodin AI, Studenyak VI, et al. Electrical properties of copper- and silver-containing superionic $(Cu_{1-x}Ag_x)_7SiS_5I$ mixed crystals with argyrodite structure. *Solid State Ionics* 2020; 345: 115183. doi: 10.1016/j.ssi.2019.115183
31. Li W, Lin S, Ge B, et al. Low sound velocity contributing to the high thermoelectric performance of Ag_8SnSe_6. *Advanced Science* 2016; 3(11): 1600196. doi: 10.1002/advs.201600196
32. Weldert KS, Zeier WG, Day TW, et al. Thermoelectric transport in Cu_7PSe_6 with high copper ionic mobility. *Journal of the American Chemical Society* 2014; 136: 12035–12040. doi: 10.1021/ja5056092
33. West DRF. *Ternary Phase Diagrams in Materials Science*, 3rd ed. CRC Press; 2019.
34. Saka H. Introduction to phase diagrams. In: *Materials Science and Engineering.* World Scientific Publishing Company; 2020.
35. Babanly MB, Mashadiyeva LF, Babanly DM, et al. Some issues of complex investigation of the phase equilibria and thermodynamic properties of the ternary chalcogenide systems by the EMF method. *Russian Journal of Inorganic Chemistry* 2019; 64(13): 1649–1671. doi: 10.1134/S0036023619130035
36. Imamaliyeva SZ, Babanly DM, Tagiev DB, et al. Physicochemical aspects of development of multicomponent chalcogenide phases having the Tl_5Te_3 structure: A review. *Russian Journal of Inorganic Chemistry* 2018; 13: 1703–1730.
37. Imamaliyeva SZ, Alakbarzade GI, Mamedov AN, et al. Modeling the phase diagrams of the Tl_9SmTe_6-Tl_4PbTe_3 and Tl_9SmTe_6-Tl_9BiTe_6 systems. *Azerbaijan Chemical Journal* 2020; 4: 12–16. doi: 10.32737/0005-2531-2020-4-12-16
38. Mammadov FM, Amiraslanov IR, Efendiyeva NN, et al. Phase diagrams of the $FeGa_2S_4$-$FeIn_2S_4$ and FeS-$FeGaInS_4$ systems. *Chemical Problems* 2019; 58–65. doi: 10.32737/2221-8688-2019-1-58-65
39. Imamaliyeva SZ, Mamedov AN, Babanly MB. Modeling the phase diagram of the Tl_9GdTe_6-Tl_4PbTe_3-Tl_9BiTe_6 system. *New Materials, Compounds and Applications* 2021; 2: 142–149. doi: 10.1007/978-3-030-64058-3_60
40. Ashirov GM. Phase equilibria in the Ag_8SiTe_6–Ag_8GeTe_6 system. *Azerbaijan Chemical Journal* 2022; 1: 89–93. doi: 10.32737/0005-2531-2022-1-89-93
41. Alverdiyev IJ, Aliev ZS, Bagheri SM, et al. Study of the $2Cu_2S+GeSe_2 \leftrightarrow 2Cu_2Se+GeS_2$ reciprocal system and thermodynamic properties of the $Cu_8GeS_{6-x}Se_x$ solid solutions. *Journal of Alloys and Compounds* 2017; 691: 255–262. doi: 10.1016/J.JALLCOM.2016.08.251
42. Aliyeva ZM, Bagheri SM, Aliev ZS, et al. The phase equilibria in the Ag_2S-Ag_8GeS_6-Ag_8SnS_6 system. *Journal of Alloys and Compounds* 2014; 611: 395–400. doi: 10.1016/j.jallcom.2014.05.112
43. Aliyeva ZM, Bagheri SM, Alverdiyev IJ, et al. Phase equilibria in the quasi-ternary system Ag_2Se-Ag_8GeSe_6-Ag_8SnSe_6. *Inorganic Materials* 2014; 50(10): 981–986. doi: 10.1134/S002016851410001X
44. Abbasova VA, Alverdiyev IJ, Mashadiyeva LF, et al. Phase relations in the Cu_8GeSe_6-Ag_8GeSe_6 system and some properties of solid solutions. *Azerbaijan Chemical Journal* 2017; 1: 30–33.
45. Alverdiyev IJ, Bagheri SM, Aliev ZM, et al. Phase equilibria in the Ag_2Se-$GeSe_2$-$SnSe_2$ system and thermodynamic properties of the solid solutions $Ag_8Ge_{1-x}Sn_xSe_6$. *Inorganic Materials* 2017; 53(8): 786–796. doi: 10.1134/S0020168517080027
46. Mashadieva LF, Alieva ZM, Mirzoeva RD, et al. Phase equilibria in the Cu_2Se–$GeSe_2$–$SnSe_2$ system. *Russian Journal of Inorganic Chemistry* 2022; 67(5): 670–682. doi: 10.1134/S0036023622050126
47. Hofmann AM. *Silver-Selenium-Silicon, Ternary Alloys*. VCH 2; 1988. pp. 559–560.
48. Venkatraman M, Blachnik R, Schlieper A. The phase diagrams of M_2X-SiX_2 (M is Cu, Ag; X is S, Se). *Thermochimica Acta* 1995; 249: 13–20. doi: 10.1016/0040-6031(95)90666-5
49. Piskach LV, Parasyuk OV, Olekseyuk ID, et al. Interaction of argyrodite family compounds with the chalcogenides of II-b elements. *Journal of Alloys and Compounds* 2006; 421: 98–104. doi: 10.1016/j.jallcom.2005.11.056
50. Boucher F, Evain M, Brec R. Single-crystal structure determination of γ-Ag_8SiTe_6 and Powder X-ray study of low-temperature α and β phases. *Journal of Solid State Chemistry* 1992; 100(2): 341–355. doi: 10.1016/0022-4596(92)90109-9
51. Emsley J. *The Elements*, 3rd ed. Oxford University Press; 1998. p. 300.
52. International Centre for Diffraction Data. ICDD.PDF-2012. Available online: https://www.icdd.com/ (accessed on 28 July 2023).